EXPRESSION OF A SECRETABLE, CELL-PENETRATING CDKL5 PROTEIN ENHANCES THE EFFICACY OF AAV VECTOR-MEDIATED GENE THERAPY FOR CDKL5 DEFICIENCY DISORDER.

Giorgio Medici*[1], Marianna Tassinari*[1], Giuseppe Galvani[1], Stefano Bastianini[1], Laura Gennaccaro[1], Manuela Loi[1], Claudia Fuchs[1], Nicola Mottolese[1], Sara Alvente[1], Chiara Berteotti[1], Helen Rappe Baggett[3], Giovanna Zoccoli[1], Maurizio Giustetto[2], Alysson Muotri[6], Hiroyuki Nakai[3,4,5], Stefania Trazzi[1], and Elisabetta Ciani[1]

[1] Department of Biomedical and Neuromotor Science, University of Bologna, Bologna, Italy.
[2] Department of Neuroscience "Rita Levi Montalcini", University of Turin, Turin, Italy
[3, 4] Departments of Molecular and Medical Genetics and Molecular Immunology and Microbiology, Oregon Health & Science University, Portland, OR 97239, USA.
[5] Division of Neuroscience, Oregon National Primate Research Center, Beaverton, OR 97006, USA.
[6] University of California San Diego, School of Medicine, Department of Pediatrics/Rady Children's Hospital-San Diego, Department of Cellular & Molecular Medicine, Kavli Institute for Brain and Mind, Archealization Center (ArchC), Center for Academic Research and Training in Anthropogeny (CARTA), La Jolla, CA 92037, USA.
Authors labeled with one asterisk contributed equally to the work.

Corresponding authors:
Elisabetta Ciani, Department of Biomedical and Neuromotor Sciences, Piazza di Porta San Donato 2, 40126 Bologna, Italy. Tel +39 0512091773; Fax +39 0512091737; e-mail: elisabetta.ciani@unibo.it; Stefania Trazzi, Department of Biomedical and Neuromotor Sciences, Piazza di Porta San Donato 2, 40126 Bologna, Italy. Tel +39 0512091743; Fax +39 0512091737; e-mail: stefania.trazzi3@unibo.it

---

ABSTRACT

No therapy is currently available for CDKL5 (cyclin-dependent kinase-like 5) deficiency disorder (CDD), a severe neurodevelopmental disorder caused by mutations in the CDKL5 gene. Although delivery of a wild-type copy of the mutated gene to cells represents the most curative approach for a monogenic disease, proof-of-concept studies highlight significant efficacy caveats for brain gene therapy. Herein, we used a secretable TATk-CDKL5 protein to enhance the efficiency of a gene therapy for CDD. We found that, although AAVPHP.B_Igk-TATk-CDKL5 and AAVPHP.B_CDKL5 vectors had similar brain infection efficiency, the AAVPHP.B_Igk-TATk-CDKL5 vector led to a higher CDKL5 protein replacement due to secretion and transduction of the TATk-CDKL5 protein into the neighboring cells. Importantly, *Cdkl5* KO mice treated with the AAVPHP.B_Igk-TATk-CDKL5 vector showed a behavioral and neuroanatomical improvement in comparison with vehicle-treated *Cdkl5* KO mice or *Cdkl5* KO mice treated with the AAVPHP.B_CDKL5 vector, indicating that a gene therapy based on a secretable recombinant TATk-CDKL5 protein is more effective at compensating *Cdkl5*-null brain defects than gene therapy based on the expression of the native CDKL5.

INTRODUCTION

CDKL5 (cyclin-dependent kinase-like 5) deficiency disorder (CDD) is a severe X-linked neurodevelopmental disease caused by mutations in the *CDKL5* gene, which lead to a lack of CDKL5 protein expression or function. CDD mainly affects girls and is characterized by early-onset epileptic seizures, hypotonia, intellectual disability, motor and visual impairment, and, in some cases, respiratory dysregulation [1-6]. Although pharmacological treatments are used to control seizures, there is currently no cure or effective treatment to ameliorate cognitive and behavioral symptoms for CDD. Animal models of CDKL5 disorder, *Cdkl5* knockout (KO) mice [7-9], recapitulate different features of CDD, exhibiting severe impairment in learning and memory, visual and respiratory deficits, and motor stereotypies [7,8,10-12] and, therefore, they are a good model with which to study the positive effects of therapeutic strategies.

In theory, for a monogenic disease such as CDD, the delivery of a wild-type copy of the mutated gene to cells which lack functional protein represents the most curative approach. Using AAV, advancements in global central nervous system (CNS) gene delivery have accelerated to the point that treatments for neurodevelopmental disorders, such as lysosomal storage disease, Rett Syndrome, CDD, Fragile X, and autism seem within reach [13]. However, gene therapy is not without risks for humans. The major caveat regards the low efficiency of gene delivery to the CNS by viral vectors that requires large vector doses, and consequently, brings the risk of immune reaction, as was the case in human clinical trials for hemophilia B [14,15]. Moreover, the new gene might be inserted into the DNA in the wrong location, possibly causing harmful mutations to the DNA or even cancer, as shown in rodent studies [16]. If the protein produced by the viral vector-infected cells can be secreted and enter into neighboring cells, this will amplify the effect of the gene therapy because, even if the transduced cells are low in number, they will become a "factory" for the production of the therapeutic protein, supplying therapeutic molecules to neighboring cells. In this scenario, the efficiency of gene delivery does not necessarily need to be high. This decreases the risk of insertional mutagenesis and toxic side effects connected with large vector doses.
We recently created an IgK-TATk-CDKL5 fusion construct and found that, in view of the properties of the Igk-chain leader sequence, the TATk-CDKL5 protein produced by infected cells is secreted via constitutive secretory pathways [17]. Importantly, due to the transduction property of the TATk peptide, the secreted CDKL5 protein is internalized by cells, maintaining its native biological activity [17].
Here we compared the effects of a CDKL5 gene therapy with an IgK-TATk-CDKL5 gene therapy in a *Cdkl5* KO mouse model to validate whether the Igk-TATk-CDKL5 approach, that enhances the biodistribution of the therapeutic CDKL5 kinase from genetically-corrected cells to non-corrected cells via a cross-correction mechanism, significantly enhances the therapeutic efficacy.

RESULTS

Production of a secretable AAVPHP.B_Igk-TATk-CDKL5 vector for gene therapy

To express the IgK-TATk-CDKL5 and CDKL5 proteins by means of AAV vector-mediated gene delivery, an Igk-TATk-CDKL5 and CDKL5 gene expression cassette [17] under the control of a strong, long-term, and ubiquitous expression promoter [18] was inserted into the AAV vector plasmid. The efficiency of the newly-constructed AAV vectors to express CDKL5 and Igk-TATk-CDKL5 proteins in neurons was confirmed after primary hippocampal neuron infection (Fig. 1A). Igk-TATk-CDKL5 showed a different expression pattern compared to CDKL5, with a more cytoplasmic distribution (Fig. 1A,B) that suggests the presence of protein secretion via the constitutive secretory pathways. We confirmed

efficient TATk-CDKL5 protein secretion using western blot analysis (Fig. 1C). TATk-CDKL5, but not CDKL5 protein, was detected in the culture medium of HEK293T cells transfected with the AAVPHP.B_Igk-TATk-CDKL5 or the AAVPHP.B_CDKL5 vector plasmid DNA (Fig. 1C). To investigate whether neurons are transduced by secreted TATk-CDKL5 protein, hippocampal neurons were co-cultured, using transwells (Fig. 1D), with HEK293T cells transfected with the AAV-Igk-TATk-CDKL5 or the AAV-CDKL5 plasmid. After 48 h of co-culture, TATk-CDKL5 protein was efficiently internalized by hippocampal neurons (Fig. 1D), while, as expected, no CDKL5-positive neurons were present (data not shown).
The efficiency of TATk-CDKL5 protein transduction in the brain was analyzed in *Cdkl5* -/Y mice intravenously injected with AAVPHP.B_Igk-TATk-CDKL5 or AAVPHP.B_CDKL5 vector and sacrificed 2 months after the injection. Although the AAVPHP.B_Igk-TATk-CDKL5 vector showed a similar infection efficiency, assessed by vector genome copy numbers in the brain, in comparison with the AAVPHP.B_CDKL5 vector (Supplementary Table 1A), and induced similar *CDKL5* mRNA levels in the brains and livers of treated mice (Supplementary Table 1B), we found that the AAVPHP.B_Igk-TATk-CDKL5 vector led to a higher CDKL5 protein replacement (Fig. 2). Based on our demonstration using an in vitro system that the Igk-TATk-CDKL5 protein can be secreted from a factory cell via the Igk signal peptide and enter neighboring cells via the TATk cell-penetrating peptide, it is most likely that more efficient CDKL5 replacement with Igk-TATk-CDKL5 than the control CDKL5 is mediated by a cross-correction mechanism.

Effect of gene therapy with AAVPHP.B_Igk-TATk-CDKL5 or AAVPHP.B_CDKL5 vector on behavior in *Cdkl5* KO mice

To compare the effects of a gene therapy with the AAVPHP.B_CDKL5 vector or the AAVPHP.B_Igk-TATk-CDKL5 vector, adult *Cdkl5* KO male mice were administered with AAV vector at a dose of 10e12 vg per mouse via intracarotid injection. To compare the effectiveness of the two vectors, we used a vector dose that resulted in 15-35% of cells being infected in the CNS (Supplementary Fig. 1A,B). The effects of treatment were evaluated 60 days post-injection (Supplementary Fig. 2A). A group of vehicle-treated *Cdkl5* KO (-/Y) and wild-type (+/Y) mice were used as controls for behavioral tests. Importantly, no changes in terms of body weight, sleep pattern, or microglial cell number were observed in vector-treated *Cdkl5* KO mice compared to age-matched vehicle-treated mice (Supplementary Fig. 2B-D), indicating that viral infection and secreted CDKL5 protein did not affect animal well-being and/or cause an inflammatory response.
Loss of Cdkl5 function in *Cdkl5* KO mice is associated with autistic-like (ASD-like) phenotypes, analyzed through home-cage social behaviors (marble burying and nest building ability) [19]. *Cdkl5* KO (-/Y) mice buried a significantly lower number of marbles and showed a reduced nest building ability compared to wild-type (+/Y) mice (Fig. 3A,B). Sixty days after treatment with AAVPHP.B_Igk-TATk-CDKL5 vector *Cdkl5* KO mice buried a higher number of marbles compared to vehicle-treated and AAVPHP.B_CDKL5-treated *Cdkl5* KO mice (Fig. 3A). Similarly, nest building ability was improved only in *Cdkl5* KO mice treated with AAVPHP.B_Igk-TATk-CDKL5 vector (Fig. 3B).
Stereotypic movements characterize *Cdkl5* KO mice [8,19] and CDD patients [20]. In order to examine the effect of gene therapy on motor stereotypies, mice were tested for hindlimb clasping (Fig. 3C). Unlike wild-type (+/Y) mice, vehicle-treated and AAVPHP.B_CDKL5-treated *Cdkl5* KO (-/Y) mice spent a lot of time in the clasping position (Fig. 3C). *Cdkl5* KO mice treated with AAVPHP.B_Igk-TATk-CDKL5 vector showed a decrease in clasping (Fig. 3C), indicating that gene therapy with Igk-TATk-CDKL5 has a greater positive impact on the stereotypic behavior that is due to loss of Cdkl5 expression.
We assessed motor function of treated *Cdkl5* KO mice in the open-field test. The elevated locomotor activity (longer distance traveled with a higher average speed; Fig. 3D) that characterizes *Cdkl5* KO

mice was improved by treatment with AAVPHP.B_Igk-TATk-CDKL5 vector (Fig. 3D), while no improvement was observed in mice treated with AAVPHP.B_CDKL5 vector.
Learning and memory were evaluated using the Barnes maze test, a cognitive paradigm in which *Cdkl5* KO mice are documented to be impaired [21]. A significative improvement in learning was observed only in *Cdkl5* KO mice treated with AAVPHP.B_Igk-TATk-CDKL5 vector (Fig. 3E). The latency that animals have before finding the escape box were assessed by the probe trial on the 4th day, confirming the spatial memory impairment of *Cdkl5* KO mice (Fig. 3F). No memory improvement was observed in *Cdkl5* KO mice treated with AAVPHP.B_Igk-TATk-CDKL5 or AAVPHP.B_CDKL5 vector (Fig. 3F).
A breathing disturbance during sleep in *Cdkl5* KO mice was recently described [17,19,22]. Using whole-body plethysmography, we found that treatment with both AAVPHP.B_CDKL5 and AAVPHP.B_Igk-TATk-CDKL5 vectors led to a drastic reduction in the number of apneas during REM sleep that became similar to that of wild-type mice (Fig. 3G). In contrast, an improvement was not achieved during NREM sleep (Fig. 3G).

Effect of gene therapy with AAVPHP.B_Igk-TATk-CDKL5 or AAVPHP.B_CDKL5 vector on dendritic hypotrophy and connectivity in the hippocampus of *Cdkl5* KO mice

Dendritic arborization was found to be reduced in cortical and hippocampal pyramidal neurons of *Cdkl5* KO mice [8,11,23,24]. In addition, *Cdkl5* KO mice exhibit a deficit in dendritic spine structure and stabilization [11,23-26] and a reduction in the number of PSD-95-positive puncta [17,24], which indicates loss of excitatory synaptic contacts. In order to establish the effect of gene therapy on dendritic pattern, we evaluated the dendritic length and spine density of CA1 pyramidal neurons (Fig. 4). In *Cdkl5* -/Y mice treated with AAVPHP.B_Igk-TATk-CDKL5 vector the length of both apical and basal dendrites was recovered compared to vehicle-treated and AAVPHP.B_CDKL5-treated *Cdkl5* KO mice (Fig. 4A,C), an improvement which may be mainly attributable to a recovery in the number of branches (Fig. 4B,C). Unlike in AAVPHP.B_CDKL5-treated *Cdkl5* -/Y mice, we found a recovery of spine density in *Cdkl5* -/Y mice treated with AAVPHP.B_Igk-TATk-CDKL5 vector in comparison with vehicle-treated *Cdkl5* -/Y mice (Fig. 4D,F). The percentage of mature spines was restored in *Cdkl5* KO mice treated with AAVPHP.B_Igk-TATk-CDKL5 vector (Fig. 4E), and it was only partially recovered in *Cdkl5* KO mice treated with AAVPHP.B_CDKL5 (Fig. 4E). Similarly, the number of PSD-95 puncta was restored in AAVPHP.B_Igk-TATk-CDKL5 treated *Cdkl5* -/Y mice (Fig. 4G,H), while only a partial improvement was present in *Cdkl5* KO mice treated with AAVPHP.B_CDKL5 (Fig. 4G,H).

Effect of gene therapy with AAVPHP.B_Igk-TATk-CDKL5 or AAVPHP.B_CDKL5 vector on neuronal survival and microglia activation in *Cdkl5* -/Y mice

Cdkl5 KO mice are characterized by decreased survival of hippocampal neurons [27,28], and by an increased microglial activation [29]. *Cdkl5* KO mice treated with AAVPHP.B_Igk-TATk-CDKL5 vector showed a higher number of Hoechst-positive nuclei and NeuN-positive pyramidal neurons in the CA1 layer (Fig. 5A-C) in comparison with vehicle- or AAVPHP.B_CDKL5-treated *Cdkl5* -/Y mice, indicating that a gene therapy with Igk-TATk-CDKL5 has a greater positive impact on the impaired neuronal survival that is due to loss of Cdkl5 expression. Similarly, a reversal of the inflammatory status, with a reduction in microglial soma size compared to the control levels, was present only in *Cdkl5* KO mice treated with AAVPHP.B_Igk-TATk-CDKL5 vector (Fig. 5D,E).

Evaluation of the efficiency of AAV vector transduction and CDKL5 protein biodistribution

To quantify and compare the efficiency of gene transfer between AAVPHP.B_Igk-TATk-CDKL5 and AAVPHP.B_CDKL5 vectors, we assessed vector genome copy numbers per cell in several brain

regions via qPCR. We found that AAVPHP.B_Igk-TATk-CDKL5 and AAVPHP.B_CDKL5 vectors had the same brain transduction efficiency, regardless of the tropism of various brain regions (Fig. 6A).
By comparing the *CDKL5* mRNA levels in treated *Cdkl5* KO mice versus those of wild-type mice we found that the levels in treated mice were much lower than those of wild-type mice in almost all the brain regions analyzed (Fig. 6B,C), indicating only a partial recovery of CDKL5 expression in *Cdkl5* KO mice. Only in the brainstem, a brain structure with relatively low CDKL5 physiological levels (Fig. 6B), did the *CDKL5* mRNA reach the levels of wild-type mice, even exceeding them (Fig. 6C), suggesting a recovery of CDKL5 expression in this brain region. The low level of *CDKL5* expression in the brains of treated *Cdkl5* KO mice was confirmed by western blot analysis (Supplementary Fig. 3A) and by the slight increase in the phosphorylation levels of the direct CDKL5 target, EB2 (Supplementary Fig. 3B).
Notably, although the AAVPHP.B_Igk-TATk-CDKL5 vector showed a similar infection efficiency in comparison with the AAVPHP.B_CDKL5 vector (Fig. 6A), which is reflected in similar CDKL5 and TATk-CDKL5 expression levels (Supplementary Fig. 3A), we found that the AAVPHP.B_Igk-TATk-CDKL5 vector led to a higher CDKL5-positive immunoreactivity in the brains of vector-treated *Cdkl5* KO mice (Fig. 6C, Supplementary Fig. 4), suggesting the occurrence of protein replacement not only in AAV vector-infected cells but also in non-infected neighboring cells by a cross-correction mechanism mediated by the secretable, cell-penetrating TATk-CDKL5 protein.

DISCUSSION

Many chronic neurological diseases do not respond to small molecule therapeutics, and have no effective therapy. Accordingly, no therapies are presently available for the improvement of the neurological phenotypes associated with CDKL5 deficiency disorder. Gene therapy offers the promise of an effective cure for both genetic and acquired brain disease. However, delivering genetic material efficiently to the CNS still remains a hurdle when developing efficacious gene therapy strategies for CNS disorders characterized by widespread neuropathology in several brain regions. Our study provides novel evidence that a gene therapy approach based on a vector carrying the Igk-TATk-CDKL5 transgene provides, by cross-correction, an increased protein biodistribution and therapeutic efficacy compared to the same vector carrying only CDKL5. We demonstrated that *Cdkl5* KO mice treated with AAVPHP.B_Igk-TATk-CDKL5 vector underwent a higher neurodevelopmental and behavioral improvement than mice treated with AAVPHP.B_CDKL5 vector. Importantly, no toxic effects, including immunogenicity problems related to the secreted TATk-CDKL5 protein, were observed in AAVPHP.B_Igk-TATk-CDKL5 treated mice, indicating the safety of this approach. These promising results suggest that a gene therapy with the Igk-TATk-CDKL5 transgene is an effective approach to treat CDD.

Following AAVPHP.B_CDKL5 vector delivery, *Cdkl5* KO mice did not exhibit improvement in behavior in comparison with vehicle-treated mice. The poor therapeutic effect of a gene therapy with only CDKL5 has previously been reported [30] and was attributed to the necessity of a more robust brain transduction to ameliorate behavioral deficits in this mouse model [31]. Noteworthy, we found that the secretable TATk-CDKL5 protein amplifies the therapeutic effect compared to the CDKL5 alone. With the same infection efficacy as that of the AAVPHP.B_CDKL5 vector, a gene therapy with AAVPHP.B_Igk-TATk-CDKL5 was sufficient to improve various behavioral defects in the *Cdkl5* KO mouse, such as innate behaviors and motor performance. Albeit in a more marginal way, hippocampal-dependent learning and memory were improved. The lesser therapeutic effect may

be attributed to the lower number of viral copies reaching the hippocampus compared to other brain regions such as the cortex, striatum and brainstem. The correlation between levels of CDKL5 re-expression and effectiveness of the gene therapy was confirmed by the finding that in the brainstem, where the CDKL5 endogenous levels are lower than in the rest of the brain [32], treatment with either AAVPHP.B_CDKL5 or AAVPHP.B_Igk-TATk-CDKL5 vectors led to an higher CDKL5 re-expression than in the other brain regions, as suggested by the mRNA levels. Accordingly, REM sleep apnea occurrence in *Cdkl5* KO mice was restored by either CDKL5 or TATk-CDKL5 expression. On the other hand, the lack of effect on the number of apneas during NREM sleep suggests that a complex behavior such as sleep breathing requires the involvement of different brain regions and, therefore, a broader CDKL5 re-expression.
As an anatomical substrate of the ameliorated behavioral performance, in AAVPHP.B_Igk-TATk-CDKL5-treated *Cdkl5* KO mice we found that their impaired dendritic and synaptic development was restored, as was neuronal survival in the hippocampus. In contrast, the lack of behavioral improvement in *Cdkl5* KO mice treated with AAVPHP.B_CDKL5 may be accounted for by the reduced effect of treatment on neuronal survival and dendritic development. Similarly, microglia over-activation, a recently described alteration in the brains of *Cdkl5* KO mice [29], is inhibited only by treatment with AAVPHP.B_Igk-TATk-CDKL5, further supporting the amplified therapeutic effect of the secretable TATk-CDKL5 protein. The reason why the restoration of several anatomical defects in the hippocampus of AAVPHP.B_Igk-TATk-CDKL5-treated *Cdkl5* KO mice does not induce the full recovery of hippocampus-dependent cognitive abilities may be attributable to the complex and intricate *in vivo* brain function which goes beyond structural restorations.

Interestingly, we observed unexpected inconsistency between the high viral copy number per cell and the low *CDKL5* mRNA and protein levels. The finding that at the same viral particle dose of 10^{12} vg per mouse, the number of GFP-positive cells is much higher than that of CDKL5-positive cells in the brains of mice injected with the Igk-TATk-CDKL5 or CDKL5 vector suggests a low half-life of the delivered CDKL5, either at the transcript or protein level. The hypothesis of *CDKL5* mRNA instability is in agreement with a recent finding showing that the lack of a long 3'-UTR sequence destabilizes *Mecp2* mRNA, significantly reducing its relative half-time [33]. In addition, it was found that viral mRNA, in contrast to endogenous mRNA, was not actively translated by ribosomes, further underscoring the importance of complex endogenous regulatory elements for Mecp2 protein expression [33]. Similarly, we found that, while the *CDKL5* mRNA levels suggest a recovery of CDKL5 expression in the brainstem, the *CDKL5* expression was much lower compared to wild-type mice, indicating that CDKL5 protein levels correlate poorly with mRNA levels. Future studies are needed to characterize regulatory elements of the *CDKL5* mRNA and to design a CDKL5 transgene cassette that would be useful to obtain higher CDKL5 protein levels. However, it was demonstrated that even a modest 5-10% re-expression of MeCP2 has a promising therapeutic effect on the RTT phenotype in a mouse model of RTT [34]. Although the actual quantity of CDKL5 required to achieve therapeutic efficacy is not known, we recently demonstrated, using a protein substitution therapy approach with a TATk-CDKL5 fusion protein [17], that the amount of CDKL5 protein necessary to rescue neurological phenotypes of a mouse model of CDD is very small (50 ng of protein per day [17]). Here we confirmed that the low CDKL5 levels re-expressed in the brains of AAV vector-treated *Cdkl5* KO mice are sufficient to improve CDD phenotypes if supported by an increased biodistribution due to the properties of the Igk-TATk fusion protein.

This study has provided a first proof-of-principle that an innovative gene therapy approach based on the unique advantages of the IgK-TATk-CDKL5 transgene is highly efficient in improving neurodevelopmental and behavioral impairments in a mouse model of CDD. Such promising results

imply that this approach may become a powerful tool for the cure of CDD, and could open avenues to the development of gene therapy for other monogenic diseases based on the unique and compelling properties of the Igk-TATk-fusion protein approach.

MATERIALS AND METHODS

Cloning of viral plasmids and production of AAV vectors

To express the Igk-TATk-CDKL5, CDKL5, and GFP proteins by means of AAV vector-mediated gene delivery, the Igk-TATk-hCDKL5$_1$, hCDKL5$_1$, or eGFP gene expression cassettes were subcloned in the backbone of pAAV-CBh-DIO-EGFP (plasmid #87168, Addgene). The designed viral cassettes between the two AAV2 inverted terminal repeats (ITRs) contain a CBh promoter (0.8 kbp), the Igk-TATk-CDKL5 (3.1 kbp), CDKL5$_1$ (2.9 kbp), or eGFP (0.7 kbp) open reading frame, followed by a WPRE and an SV40 polyadenylation signal (0.4 kbp). The TATk-CDKL5 and CDKL5 proteins were tagged with a haemagglutinin (HA)-tag. The AAV vector genomes containing the above-described expression cassettes were packaged in the AAVPHP.B capsid in HEK293 cells using an adenovirus-free triple transfection method (for details, see Supplementary material).

Cell lines and primary cultures

HEK293T cell line was maintained in Dulbecco Modified Eagle Medium (DMEM, Gibco) supplemented with 10% heat-inactivated FBS (Gibco), 2 mM of glutamine (Gibco), and antibiotics (penicillin, 100 U/mL; streptomycin, 100 µg/mL; Gibco), in a humidified atmosphere of 5% of CO2 at 37°C. Cell medium was replaced every 3 days and the cells were sub-cultured once they reached 90% confluence. Cells were transfected with designated plasmid DNA using Metafectene Easy Plus (Biontex). Forty-eight hours after transfection, cells were harvested, washed in PBS, and lysed for total protein extraction. Cell medium was also collected and 200x concentrated as described previously [17]. Cell extracts and medium were used for western blot analysis.
Primary hippocampal neuronal cultures were prepared from 1-day-old (P1) wild-type and *Cdkl5* KO mice as previously described [35]. Briefly, hippocampi were dissected from mouse brains under a dissection microscope and treated with trypsin (Gibco) for 15 min at 37°C and DNase I (Sigma-Aldrich) for 2 min at room temperature before being triturated mechanically with a fire-polished glass pipette to obtain a single-cell suspension. Cells were plated on coverslips coated with poly-L-lysine in 6-well plates and cultured in Neurobasal medium (Gibco) supplemented with B27 (Invitrogen) and glutamine (Gibco). Cells were maintained in vitro at 37°C in a 5% CO2-humified incubator.

In vitro AAV transduction

Primary hippocampal neurons were infected with AAVPHP.B_Igk-TATk-CDKL5 and AAVPHP.B_CDKL5 (MOI of 10^6) at day in vitro (DIV) 2, fixed at DIV7 with 4% paraformaldehyde + 4% sucrose in 100 mM phosphate buffer pH 7.4. Fixed cells were stained with the primary and secondary antibodies listed in Supplementary Table 2. Nuclei were counterstained with Hoechst-33342 (Sigma-Aldrich) and fluorescent images were acquired using a Nikon Eclipse Te600 microscope equipped with a Nikon Digital Camera DXM1200 ATI system (Nikon Instruments, Inc. Melville, NY, USA).

Co-culture system

For co-culture experiments, HEK293T cells were plated in a 6-well plate, while primary hippocampal neurons were plated on cover glasses. Twenty-four hours after plating, HEK293T cells were transfected with the AAV vector plasmid containing the Igk-TATk-CDKL5 or CDKL5 cassette. Twenty-

four hours after transfection, the co-culture was prepared as follows: HEK293T cells were washed twice with fresh neuronal culture medium. The cover glasses with primary hippocampal neurons (DIV5) were transferred to the HEK293T 6-well plate in an elevated position of the gel supports underneath. After 48 h of co-culturing, the cover glasses with neurons were removed; neurons were washed in PBS, fixed with 4% paraformaldehyde + 4% sucrose in 100 mM phosphate buffer pH 7.4 and processed for immunocytochemistry. The primary and secondary antibodies used are listed in Supplementary Table 2.

Animal husbandry

The mice used in this work derive from the *Cdkl5* KO strain in the C57BL/6N background developed in [8] and backcrossed in C57BL/6J for three generations. Animals were genotyped as previously described [8]. Age-matched wild-type (+/Y) littermates were used for all experiments. The day of birth was designated as postnatal day (P) zero and animals with 24 h of age were considered as 1-day-old animals (P1). Mice were housed 3–5 per cage on a 12 h light/dark cycle in a temperature- (23 °C) and humidity-controlled environment with standard mouse chow and water *ad libitum*. The animals' health and comfort were controlled by the veterinary service. All research and animal care procedures were performed in accordance with the Italian and European Community law for the use of experimental animals and were approved by Bologna University Bioethical Committee. All efforts were made to minimize animal suffering and to keep the number of animals used to a minimum.

In vivo AAV delivery

Intravenous infusion - Mice were injected in the lateral tail vein with a dose of $5x10^{11}$ vg/mouse.

Intracarotid infusion - Surgery was performed under general anesthesia (ISOFLO, Esteve Spa, 1.8-2.4% in oxygen, inhalation route) with the mouse's body temperature maintained at 37°C by using a heating pad and intra-operative analgesia (10 µL of Norocarp dissolved in 1 ml of saline; 0.2 ml subcutaneously, Pfizer). All procedures were performed in sterile conditions. The tip of the catheter was flushed with sterile heparin. The isolation of the carotid artery was performed as previously described [36]. Once isolated, two silk suture threads (Softsilk 5-0) were proximally and distally placed below the arterial segment of interest. The proximal thread (posterior, close to the heart) was permanently knotted and tied while the distal one (near the bifurcation of the carotid) was only pulled by another operator to temporarily close off the artery and to keep the artery slightly taut during the insertion of the catheter. The catheter was inserted between the suture threads, close to the proximal thread, through a hole made by a 90° bent needle (25 G). After the tip of the catheter was inserted, the viral solution was infused with 50 µl/min speed. Mice were injected with a dose of 10^{12} vg/mouse. When all the amount of the solution was infused, the infusion was stopped and the catheter was gently pulled out. The threads were both tied. Finally, suture stitches and an antiseptic ointment (Betadine 10%, Viatris) were applied to the skin incision. At the end of the surgical procedure, an antibiotic solution (30 µL of Veterinary Rubrocillin, Intervet, Schering-Plow Animal Health, dissolved in 0.8 ml of sterile saline) was administered subcutaneously to prevent infections and to rehydrate the animal.

Behavioral Testing

Behavioral tests were performed 2 months after the injection. The sequence of the tests was arranged to minimize the possibility of one test influencing the subsequent evaluation of the next test, and mice were allowed to recover for 2 days between different tests. Mice were allowed to habituate to the testing room for at least 1 h before the test, and testing was always performed at the same time of day. Behavioral studies were carried out on the saline-injected *Cdkl5* +/Y and *Cdkl5*

-/Y mice groups and AAV-injected *Cdkl5* -/Y mice groups. A total of 87 animals divided into three independent test cohorts were used. The first test cohort consisted of 34 animals (*Cdkl5* +/Y + vehicle n = 10, *Cdkl5* -/Y + vehicle n = 6, *Cdkl5* -/Y + AAVPHP.B_CDKL5 n = 10, and *Cdkl5* -/Y + AAVPHP.B_Igk-TATk-CDKL5 n = 8) that were tested with the following assays: marble burying, nesting test, hindlimb clasping, open field, Barnes maze. The second cohort consisted of 34 animals (*Cdkl5* +/Y + vehicle n = 4, *Cdkl5* -/Y + vehicle n = 10, *Cdkl5* -/Y + AAVPHP.B_CDKL5 n = 10, and *Cdkl5* -/Y + AAVPHP.B_Igk-TATk-CDKL5 n = 10) that were tested with the following assays: marble burying, nesting test, hindlimb clasping, open field. The third cohort consisted of 19 animals (*Cdkl5* +/Y + vehicle n = 6, *Cdkl5* -/Y + AAVPHP.B_CDKL5 n = 6, and *Cdkl5* -/Y + AAVPHP.B_Igk-TATk-CDKL5 n = 7) that were tested with the following assays: marble burying, nesting test, hindlimb clasping, open field, Barnes maze. See Supplementary material for detailed behavioral methods.

Non-invasive assessment of sleep and breathing pattern

Hypnic and respiratory phenotypes of mice were assessed non-invasively with a validated technique based on whole-body plethysmography (WBP) [22,37]. Briefly, each mouse was placed inside a WBP chamber flushed with air at 1.5 l/h for the first 8 h of the light period. The respiratory (WBP chamber pressure) signal was continuously recorded together with chamber humidity and temperature, digitized, and stored at 128 Hz, 4 Hz, and 4 Hz, respectively. The system was calibrated with a 100 µl micro-syringe (Hamilton, Reno, USA) at the end of each recording. The states of wakefulness, non-rapid-eye-movement sleep (NREMS), and rapid-eye-movement sleep (REMS) were scored based on inspection of the raw WBP signal with the investigators blind to the animal's genotype. Quantitative analysis of breathing was restricted to stable sleep episodes ≥ 12 s because of the frequent occurrence of movement artefacts during wakefulness. Apneas were automatically detected as breaths with instantaneous total breath duration (TTOT) > 3 times; the average TTOT for each mouse and sleep state, and detection accuracy were checked on raw recordings.

Immunohistochemistry procedures

Mice were sedated with isoflurane (2% pure oxygen) and sacrificed for cervical dislocation. The brains were quickly removed and cut along the midline. The two hemispheres were fixed separately by immersion in a solution of 4% paraformaldehyde in 100 mM phosphate buffer (pH 7.4) for 48 h and subsequently stored in 20% sucrose for another 24 h, before being frozen in dry ice and kept at - 80 °C. The hemispheres were then cut with a freezer microtome into 30 µm-thick coronal sections which were serially collected in a 96-well plate containing a solution consisting of 30% glycerol, 30% ethylene glycol, 0.02% sodium azide in 1X PBS. The primary and secondary antibodies used are listed in Supplementary Table 2.

For quantification of PSD-95 immunoreactive puncta, images from the CA1 layer were acquired using a LEICA TCS SL confocal microscope (LEITZ; Leica Microsystems, Wetzlar, Germany; objective 63X, NA 1.32; zoom factor = 8). Three to four sections per animal were analyzed and the number of PSD-95 immunoreactive puncta was expressed per μm^2.

For morphometric microglial cell analysis, starting from 20X magnification images of AIF-1-stained hippocampal and cortical slices, AIF-1 positive microglial cell body size was manually drawn using the Image Pro Plus measurement function, and expressed in μm^2.

Golgi staining, neuronal tracing and spine evaluation

Hemispheres were Golgi-stained using the FD Rapid GolgiStain TM Kit (FD NeuroTechnologies) as previously described [38]. Dendritic trees of Golgi-stained apical dendritic branches of CA1 field neurons were traced with a dedicated software that was custom-designed for dendritic reconstruction (Immagini Computer), interfaced with Image Pro Plus (Media Cybernetics). Dendritic

spine density was measured by manually counting the number of dendritic spines. In each mouse, 10-15 dendritic segments (segment length: 10 µm) from each zone were analyzed and spine density was expressed as the total number of spines per 10 µm. Based on their morphology, dendritic spines can be divided into two different categories that reflect their state of maturation: immature spines and mature spines. The number of spines belonging to each class was counted and expressed as a percentage.

Western Blotting

HEK293T cells transfected with plasmid DNA were lysates in Laemmli buffer supplemented with β-mercaptoethanol, sonicated and boiled at 95 °C for 10 min. Brains of treated *Cdkl5* KO mice were homogenized in ice-cold RIPA buffer supplemented with 1mM PMSF, and with 1% protease and phosphatase inhibitor cocktail (Sigma-Aldrich). Equivalent amounts of protein were subjected to electrophoresis on a 4-12% Mini-PROTEAN® TGXTM Gel (Bio-Rad) and transferred to a Hybond-ECL nitrocellulose membrane (Amersham - GE Healthcare Life Sciences). For CDKL5 detection, 80 µg of proteins were loaded on the gel. The primary and secondary antibodies used are listed in Supplementary Table 2.

Real-Time PCR

Animals were sedated with isoflurane (2% pure oxygen) and sacrificed for cervical dislocation. The brain and liver were quickly removed. Various brain regions were dissected and stored at -80 °C.

Viral biodistribution analysis - Genomic DNA (gDNA) was extracted from the brain region of interest with the NucleoSpin®Tissue Kit (Macherey-Nagel) extraction kit and 100 ng of gDNA was used as a qPCR template. For the quantification of the number of viral copies, a portion of the viral promoter CBh was amplified (Fw 5'-TACTCCCACAGGTGAGCGG-3 ', Rev 5'-GGCAGGTGCTCCAGGTAAT-3'; E=100%). For data normalization a portion of the mAgouti gene was also amplified (Fw 5'-GGCGTGGTCAGTGGTTGTG-3 ', Rev 5'-TTTAGCTTCCACTAGGTTTCCTAGAAA-3'; E=100%). For data interpolation, the calibration curves for CBh and mAgouti were generated through the quantification of serial dilutions of the AAV vector plasmid and a plasmid containing Agouti fragment, respectively. A master calibration curve for CBh and mAgouti was calculated as the mean of several calibration curves obtained from multiple runs (N = 9, for CBh; N = 12, for mAgouti) [39]. Ct values were interpolated in the master calibration curve to obtain the number of viral copies for each sample and the mAgouti copy number for internal normalization. Finally, viral copy number/cell was calculated for each sample considering the murine genomic DNA molecular weight of 3pg (6pg per diploid cells).

Analysis of AAV vector genome transcripts - Total RNA was isolated from the brains and livers of *Cdkl5* KO mice treated with vehicle, AAVPHP.B_CDKL5, or AAVPHP.B_Igk-TATk-CDKL5 with the GRS FullSample Purification Kit (GRISP) according to the manufacturer's instruction. Isolated mRNA was subjected to a DNase I treatment (GRISP), and cDNA synthesis was achieved using iScript™ Advanced cDNA Synthesis Kit (Bio-Rad), according to the manufacturer's instruction. Reverse transcriptase - PCRs were performed using SsoAdvanced Universal SYBR Green Supermix (Bio-Rad) in iQ5 Real-Time PCR Detection System (Bio-Rad). A portion of the m-hCDKL5 (Fw 5'-GACACAAGGAAACACATGAAATTG-3 ', Rev 5'-TCCACAATGTTTTCCTGCTTGA-3') and hCDKL5 (Fw 5'-GCAGACACAAGGAAACACATGA-3', Rev 5'-CAACTTTCCCCTCCGACGAA-3') sequence was amplified for the quantification of AAV vector genome transcripts. A portion of mGAPDH (Fw 5'-GAACATCATCCCTGCATCCA-3', Rev 5'-CCAGTGAGCTTCCCGTTCA-3') sequence was amplified for data normalization. The differential folds of expression were calculated using the ΔΔCt method. Values

were expressed as the fold increase in the CDKL5 expression in the cortex relative to that of the wild types.

Statistical Analysis

Results are presented as mean ± standard error of the mean (± SE), and n indicates the number of mice. Statistical analysis was performed using GraphPad Prism software (GraphPad Software, Inc., San Diego, CA). Continuos data were analyzed using the ROUT method (Q=1%) for the identification of significant outliers. All datasets were analyzed using the Shapiro-Wilk test for normality testing. Datasets with normal distribution were analyzed for significance using Student's t-test or an ordinary one-way analysis of variance (ordinary one-way ANOVA). *Post hoc* multiple comparisons were carried out using the Fisher least significant difference (Fisher's LSD) or a Tukey test. Datasets with non-parametric distribution were analyzed using the Kruskal-Wallis test. *Post hoc* multiple comparisons were carried out using Dunn's multiple comparison test or the Mann-Whitney U test. For the open field and the learning phase of the Barnes maze, statistical analysis was performed using a repeated measure two-way analysis of variance (RM two-way ANOVA). A probability level of $p<0.05$ was considered to be statistically significant.

FUNDING

This work was supported by the Telethon Foundation (grant number GGP19045 to EC and MG), by the Jérôme Lejeune Foundation, the University of Pennsylvania Orphan Disease Center (on behalf of LouLou Foundation) and the Italian parent association "CDKL5 insieme verso la cura" (grant to EC and HN).

BIBLIOGRAPHY

1 Mari, F. *et al.* CDKL5 belongs to the same molecular pathway of MeCP2 and it is responsible for the early-onset seizure variant of Rett syndrome. *Hum Mol Genet* **14**, 1935-1946, doi:10.1093/hmg/ddi198 (2005).

2 Bertani, I. *et al.* Functional consequences of mutations in CDKL5, an X-linked gene involved in infantile spasms and mental retardation. *J Biol Chem* **281**, 32048-32056, doi:10.1074/jbc.M606325200 (2006).

3 Fehr, S. *et al.* The CDKL5 disorder is an independent clinical entity associated with early-onset encephalopathy. *Eur J Hum Genet* **21**, 266-273, doi:10.1038/ejhg.2012.156 (2013).

4 Guerrini, R. & Parrini, E. Epilepsy in Rett syndrome, and CDKL5- and FOXG1-gene-related encephalopathies. *Epilepsia* **53**, 2067-2078, doi:10.1111/j.1528-1167.2012.03656.x (2012).

5 Olson, H. E. *et al.* Cyclin-Dependent Kinase-Like 5 Deficiency Disorder: Clinical Review. *Pediatr Neurol* **97**, 18-25, doi:10.1016/j.pediatrneurol.2019.02.015 (2019).

6 Demarest, S. *et al.* Severity Assessment in CDKL5 Deficiency Disorder. *Pediatr Neurol* **97**, 38-42, doi:10.1016/j.pediatrneurol.2019.03.017 (2019).

7 Wang, I. T. *et al.* Loss of CDKL5 disrupts kinome profile and event-related potentials leading to autistic-like phenotypes in mice. *Proc Natl Acad Sci U S A* **109**, 21516-21521, doi:10.1073/pnas.1216988110 (2012).

8 Amendola, E. *et al.* Mapping pathological phenotypes in a mouse model of CDKL5 disorder. *PLoS One* **9**, e91613, doi:10.1371/journal.pone.0091613 (2014).

9 Okuda, K. *et al.* CDKL5 controls postsynaptic localization of GluN2B-containing NMDA receptors in the hippocampus and regulates seizure susceptibility. *Neurobiol Dis* **106**, 158-170, doi:10.1016/j.nbd.2017.07.002 (2017).

10 Fuchs, C. *et al.* Loss of CDKL5 impairs survival and dendritic growth of newborn neurons by altering AKT/GSK-3beta signaling. *Neurobiol Dis* **70**, 53-68, doi:10.1016/j.nbd.2014.06.006 (2014).

11 Fuchs, C. *et al.* Inhibition of GSK3beta rescues hippocampal development and learning in a mouse model of CDKL5 disorder. *Neurobiol Dis* **82**, 298-310, doi:10.1016/j.nbd.2015.06.018 (2015).
12 Ren, E. *et al.* Functional and Structural Impairments in the Perirhinal Cortex of a Mouse Model of CDKL5 Deficiency Disorder Are Rescued by a TrkB Agonist. *Front Cell Neurosci* **13**, 169, doi:10.3389/fncel.2019.00169 (2019).
13 Gray, S. J. Gene therapy and neurodevelopmental disorders. *Neuropharmacology* **68**, 136-142, doi:10.1016/j.neuropharm.2012.06.024 (2013).
14 Manno, C. S. *et al.* Successful transduction of liver in hemophilia by AAV-Factor IX and limitations imposed by the host immune response. *Nat Med* **12**, 342-347, doi:10.1038/nm1358 (2006).
15 Nathwani, A. C. *et al.* Long-term safety and efficacy of factor IX gene therapy in hemophilia B. *N Engl J Med* **371**, 1994-2004, doi:10.1056/NEJMoa1407309 (2014).
16 Donsante, A. *et al.* AAV vector integration sites in mouse hepatocellular carcinoma. *Science* **317**, 477, doi:10.1126/science.1142658 (2007).
17 Trazzi, S. *et al.* CDKL5 protein substitution therapy rescues neurological phenotypes of a mouse model of CDKL5 disorder. *Hum Mol Genet* **27**, 1572-1592, doi:10.1093/hmg/ddy064 (2018).
18 Gray, S. J. *et al.* Optimizing promoters for recombinant adeno-associated virus-mediated gene expression in the peripheral and central nervous system using self-complementary vectors. *Hum Gene Ther* **22**, 1143-1153, doi:10.1089/hum.2010.245 (2011).
19 Fuchs, C. *et al.* Heterozygous CDKL5 Knockout Female Mice Are a Valuable Animal Model for CDKL5 Disorder. *Neural Plast* **2018**, 9726950, doi:10.1155/2018/9726950 (2018).
20 Bahi-Buisson, N. & Bienvenu, T. CDKL5-Related Disorders: From Clinical Description to Molecular Genetics. *Mol Syndromol* **2**, 137-152, doi:10.1159/000331333 (2012).
21 Okuda, K. *et al.* Comprehensive behavioral analysis of the Cdkl5 knockout mice revealed significant enhancement in anxiety- and fear-related behaviors and impairment in both acquisition and long-term retention of spatial reference memory. *PLoS One* **13**, e0196587, doi:10.1371/journal.pone.0196587 (2018).
22 Lo Martire, V. *et al.* CDKL5 deficiency entails sleep apneas in mice. *J Sleep Res* **26**, 495-497, doi:10.1111/jsr.12512 (2017).
23 Fuchs, C. *et al.* Treatment with the GSK3-beta inhibitor Tideglusib improves hippocampal development and memory performance in juvenile, but not adult, Cdkl5 knockout mice. *Eur J Neurosci* **47**, 1054-1066, doi:10.1111/ejn.13923 (2018).
24 Trazzi, S. *et al.* HDAC4: a key factor underlying brain developmental alterations in CDKL5 disorder. *Hum Mol Genet* **25**, 3887-3907, doi:10.1093/hmg/ddw231 (2016).
25 Della Sala, G. *et al.* Dendritic Spine Instability in a Mouse Model of CDKL5 Disorder Is Rescued by Insulin-like Growth Factor 1. *Biol Psychiatry* **80**, 302-311, doi:10.1016/j.biopsych.2015.08.028 (2016).
26 Ricciardi, S. *et al.* CDKL5 ensures excitatory synapse stability by reinforcing NGL-1-PSD95 interaction in the postsynaptic compartment and is impaired in patient iPSC-derived neurons. *Nat Cell Biol* **14**, 911-923, doi:10.1038/ncb2566 (2012).
27 Loi, M. *et al.* Treatment with a GSK-3beta/HDAC Dual Inhibitor Restores Neuronal Survival and Maturation in an In Vitro and In Vivo Model of CDKL5 Deficiency Disorder. *Int J Mol Sci* **22**, doi:10.3390/ijms22115950 (2021).
28 Gennaccaro, L. *et al.* Age-Related Cognitive and Motor Decline in a Mouse Model of CDKL5 Deficiency Disorder is Associated with Increased Neuronal Senescence and Death. *Aging and disease* (2021).
29 Galvani, G. *et al.* Inhibition of Microglia Over-activation Restores Neuronal Survival in a Mouse Model of CDKL5 Deficent Disorder. *Journal of Neuroinflammation* **Preprints**, doi:doi.org/10.21203/rs.3.rs-203260/v1 (2021).
30 Gao, Y. *et al.* Gene replacement ameliorates deficits in mouse and human models of cyclin-dependent kinase-like 5 disorder. *Brain* **143**, 811-832, doi:10.1093/brain/awaa028 (2020).
31 Benke, T. A. & Kind, P. C. Proof-of-concept for a gene replacement approach to CDKL5 deficiency disorder. *Brain* **143**, 716-718, doi:10.1093/brain/awaa055 (2020).
32 Kilstrup-Nielsen, C. *et al.* What we know and would like to know about CDKL5 and its involvement in epileptic encephalopathy. *Neural Plast* **2012**, 728267, doi:10.1155/2012/728267 (2012).

33 Luoni, M. *et al.* Whole brain delivery of an instability-prone Mecp2 transgene improves behavioral and molecular pathological defects in mouse models of Rett syndrome. *Elife* **9**, doi:10.7554/eLife.52629 (2020).
34 Carrette, L. L. G., Blum, R., Ma, W., Kelleher, R. J., 3rd & Lee, J. T. Tsix-Mecp2 female mouse model for Rett syndrome reveals that low-level MECP2 expression extends life and improves neuromotor function. *Proc Natl Acad Sci U S A* **115**, 8185-8190, doi:10.1073/pnas.1800931115 (2018).
35 Beaudoin, G. M., 3rd *et al.* Culturing pyramidal neurons from the early postnatal mouse hippocampus and cortex. *Nat Protoc* **7**, 1741-1754, doi:10.1038/nprot.2012.099 (2012).
36 Jacobs, J. D. & Hopper-Borge, E. A. Carotid artery infusions for pharmacokinetic and pharmacodynamic analysis of taxanes in mice. *J Vis Exp*, e51917, doi:10.3791/51917 (2014).
37 Bastianini, S. *et al.* Accurate discrimination of the wake-sleep states of mice using non-invasive whole-body plethysmography. *Sci Rep* **7**, 41698, doi:10.1038/srep41698 (2017).
38 Guidi, S. *et al.* Early pharmacotherapy with fluoxetine rescues dendritic pathology in the Ts65Dn mouse model of down syndrome. *Brain Pathol* **23**, 129-143, doi:10.1111/j.1750-3639.2012.00624.x (2013).
39 Sivaganesan, M., Haugland, R. A., Chern, E. C. & Shanks, O. C. Improved strategies and optimization of calibration models for real-time PCR absolute quantification. *Water Res* **44**, 4726-4735, doi:10.1016/j.watres.2010.07.066 (2010).

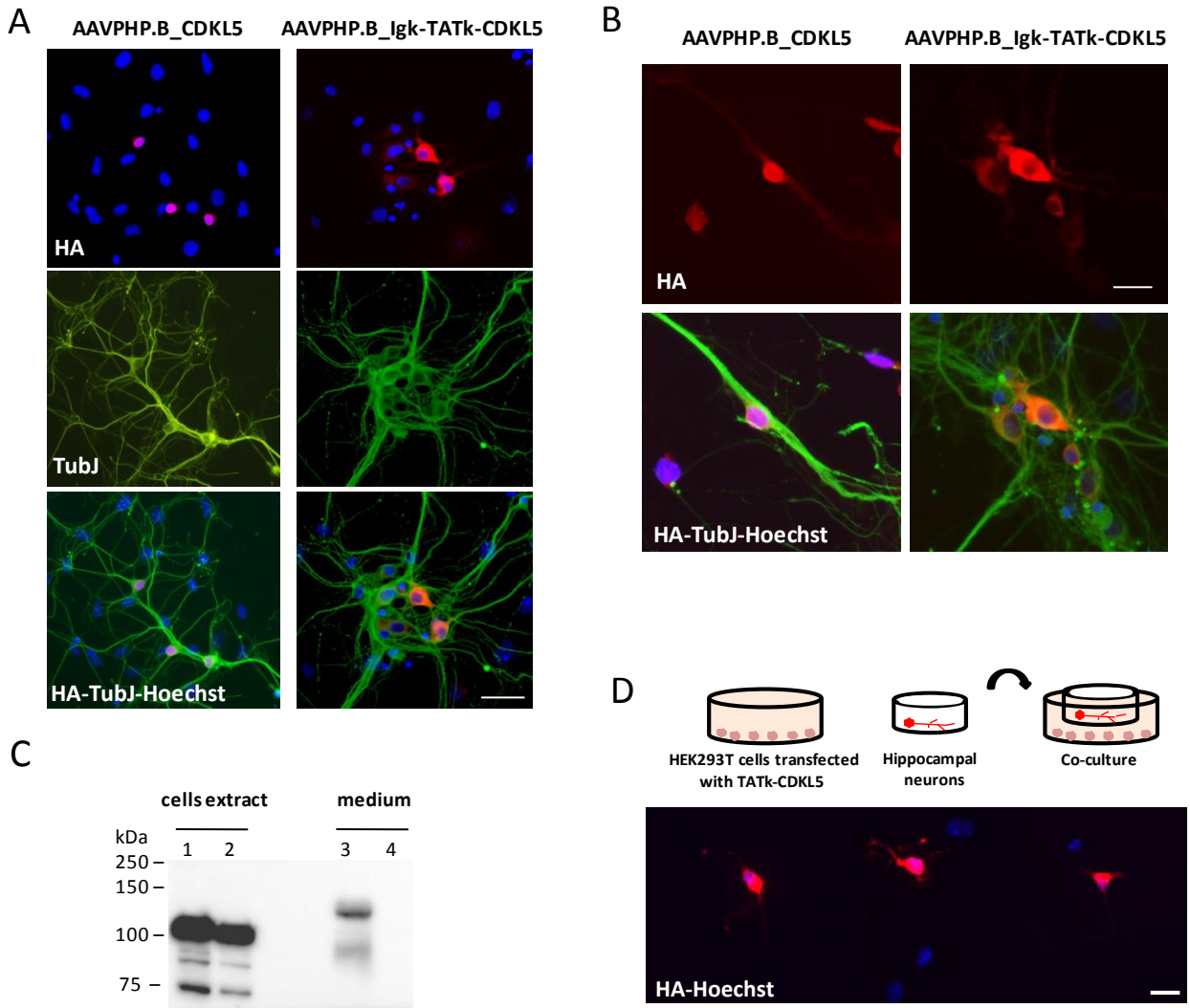

Figure 1 Secretion and transduction efficiency of the TATk-CDKL5 protein.
(A, B) Two-day (DIV2) primary hippocampal neuronal cultures from *Cdkl5* -/Y mice were infected with the AAVPHP.B_Igk-TATk-CDKL5 or the AAVPHP.B_CDKL5 vector (MOI 10^6) and fixed at DIV 7. CDKL5 and TATk-CDKL5 protein localization was assessed by immunostaining with an anti-HA antibody (red) and an anti-β III tubulin antibody (TubJ, green). Nuclei were counterstained with Hoechst. Scale bars = 25 μm (A), 10 μm (B). (C) Western blot analysis using an anti-HA antibody confirmed TATk-CDKL5 and CDKL5 protein expression in AAV vector plasmid DNA-transfected HEK293T cells (cell extract, lanes 1 and 2), and TATk-CDKL5 protein accumulation in the concentrated culture medium (lane 3), indicating that the TATk-CDKL5 protein was secreted from cells. (D) Co-culture experimental design: HEK293T cells were transfected with the AAV vector plasmid containing the Igk-TATk-CDKL5 cassette. Twenty-four hours after transfection, cover glasses with 5-day (DIV5) differentiated primary hippocampal neurons were transferred to the HEK293T 6-well plate in an elevated position. Fluorescence microscopy images showing the presence of TATk-CDKL5 protein in differentiated primary hippocampal neurons from *Cdkl5* -/Y mice co-cultured for 48 h (DIV5-DIV7) with HEK293T cells transfected with AAVPHP.B_Igk-TATk-CDKL5 plasmid. Neurons were immunostained with an anti-HA antibody (red) and nuclei were counterstained with Hoechst. Scale bar = 10 μm.

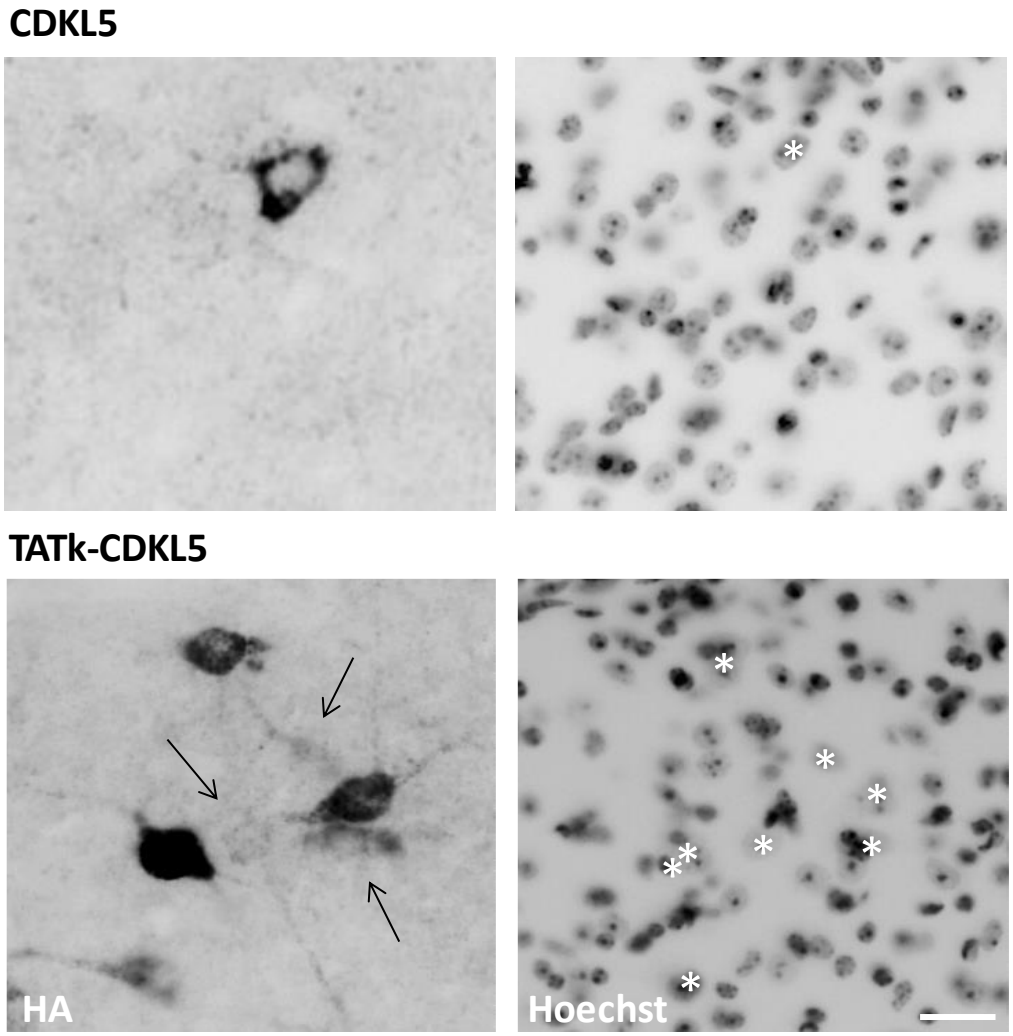

Figure 2 CDKL5 and TATk-CDKL5 protein distribution in the CNS.
Adult mice (3 months) were systemically treated (intravenous tail injection) with AAVPHP.B_CDKL5 or AAVPHP.B_Igk-TATk-CDKL5 vector, and brain samples were collected 90 days post-injection. Images show TATk-CDKL5 or CDKL5 protein localization in the striatum of treated mice 90 days post-injection. Localization of TATk-CDKL5 or CDKL5 was evaluated through immunohistochemistry using an anti-HA antibody, and nuclei were counterstained with Hoechst. Scale bar = 25 μm. The arrows indicate faintly HA-immunopositive cells; the asterisks indicate the nuclei of all the immunolabeled cells.

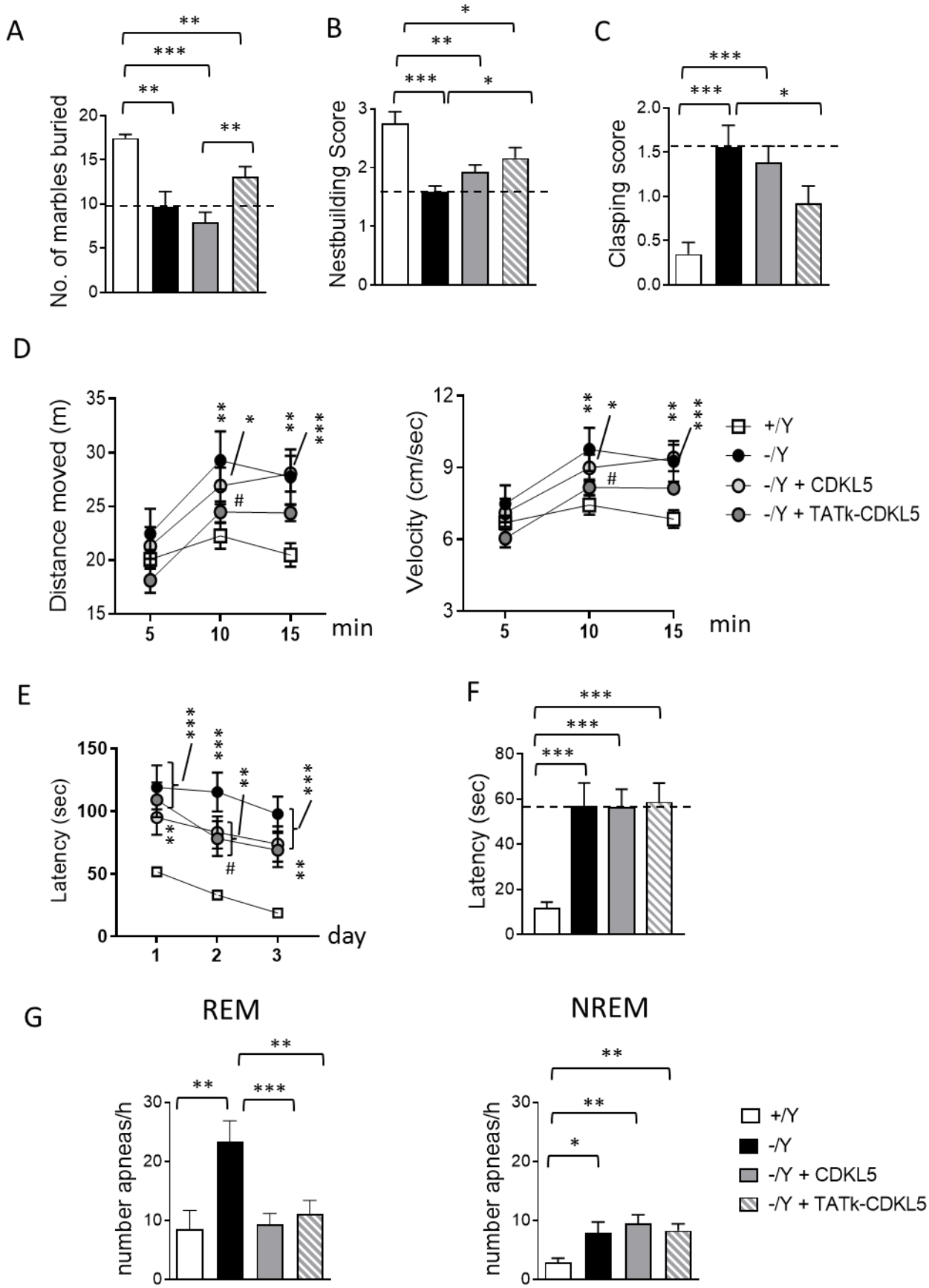
A
No. of marbles buried
B
Nestbuilding Score
C
Clasping score
D
Distance moved (m)
min
Velocity (cm/sec)
min
+/Y
-/Y
-/Y + CDKL5
-/Y + TATk-CDKL5
E
Latency (sec)
day
F
Latency (sec)
G
REM
NREM
number apneas/h
number apneas/h
+/Y
-/Y
-/Y + CDKL5
-/Y + TATk-CDKL5

Figure 3 Effect of CDKL5 and TATk-CDKL5 proteins on behavior in *Cdkl5* KO mice.
(A, B) Autistic-like features in treated *Cdkl5* KO mice. Number of marbles buried (A) and nest quality (B) of wild-type mice (+/Y, n = 20) and *Cdkl5* KO mice (-/Y, n = 6 (A); n = 16 (B)) and of *Cdkl5* -/Y mice 60 days from treatment with AAVPHP.B_CDKL5 (n = 26) or AAVPHP.B_Igk-TATk-CDKL5 (n = 25). (C) Hind-limb clasping score during a 2 min interval in wild-type mice (+/Y, n = 20) and *Cdkl5* KO mice (-/Y, n = 16), and in *Cdkl5* -/Y mice 60 days after treatment with AAVPHP.B_CDKL5 (n = 26) or AAVPHP.B_Igk-TATk-CDKL5 (n = 25). (D) Total distance traveled (left graph) and average locomotion velocity (right graph) of wild-type mice (+/Y, n = 20) and Cdkl5 KO mice (-/Y, n = 16), and of *Cdkl5* -/Y mice treated with AAVPHP.B_CDKL5 (n = 26) or AAVPHP.B_Igk-TATk-CDKL5 (n = 25), during a 15 min open field test (E,F). Spatial learning and memory assessed using the Barnes Maze in wild-type mice (+/Y, n = 16) and *Cdkl5* KO mice (-/Y, n = 11), and in *Cdkl5* -/Y mice treated with AAVPHP.B_CDKL5 (n = 16) or AAVPHP.B_Igk-TATk-CDKL5 (n = 14). Graphs show the mean latency to find the target hole during the 3-day learning period (E) and the latency to find the target hole (F), on the probe day (day 4). (G) Sleep apnea occurrence rate in treated *Cdkl5* KO mice was assessed using whole-body plethysmography. Sleep apnea occurrence in vehicle-treated wild-type (+/Y, n = 9) and *Cdkl5* KO (-/Y, n = 7) mice, and in *Cdkl5* KO mice treated with AAVPHP.B_CDKL5 (n = 16) or AAVPHP.B_Igk-TATk-CDKL5 (n = 15), during rapid eye movement (REM) sleep and non-rapid eye movement (NREM) sleep. Values are presented as means ± SE. *$p < 0.05$; **$p < 0.01$; ***$p < 0.001$ (datasets in A,B, C and F, Dunn's test after Kruskall-Wallis; datasets in G, Fisher's LSD test after one-way ANOVA). Values in (D, E) are presented as means ± SE. *$p < 0.05$; **$p < 0.01$; ***$p < 0.001$ compared to the vehicle-treated wild-type condition; #$p < 0.05$ as compared to the vehicle-treated *Cdkl5* -/Y samples (Fisher's LSD test after RM two-way ANOVA).

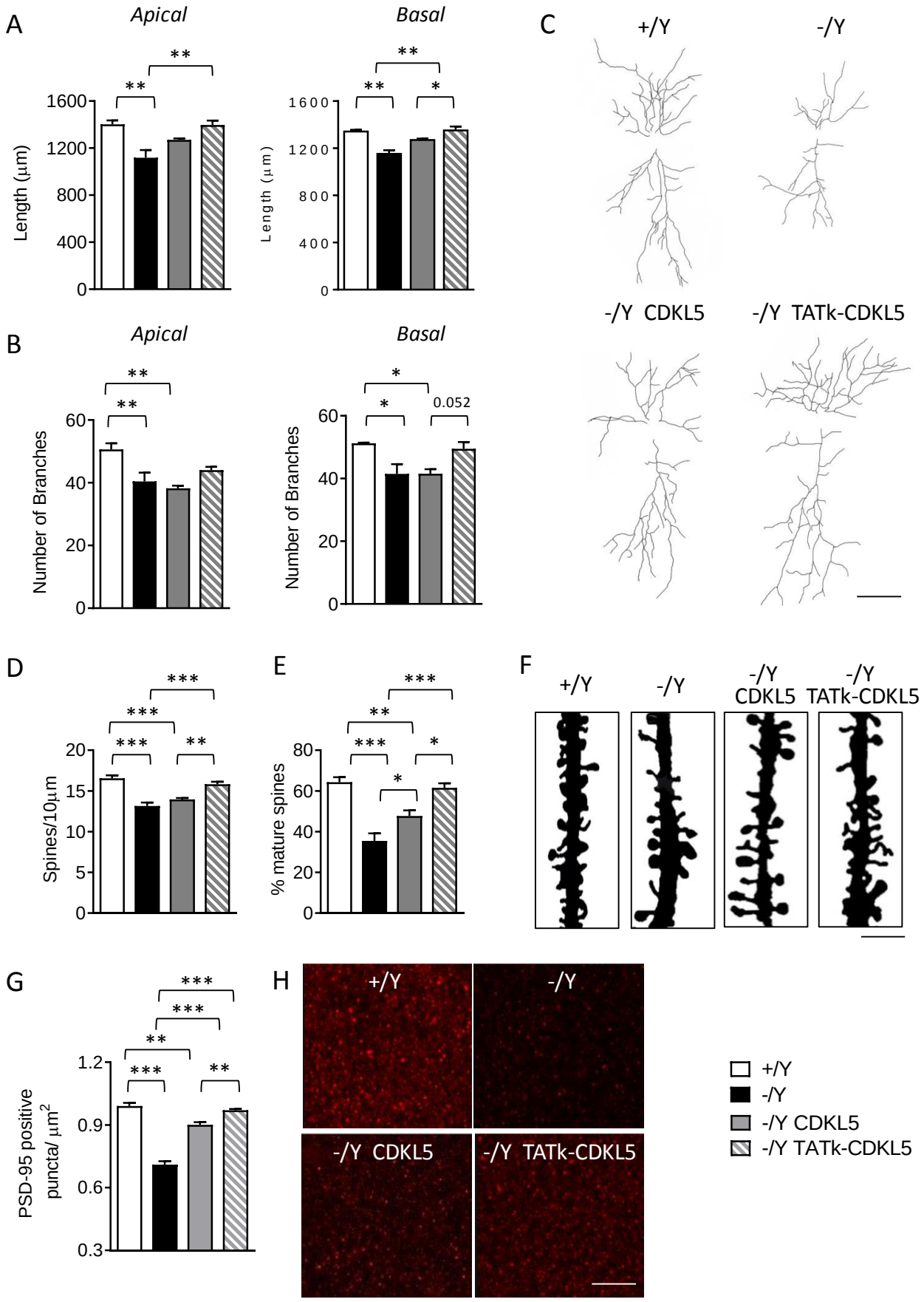
A
Apical
Basal
Length (µm)
1600
1200
800
400
0
**
*
B
Number of Branches
60
40
20
0
0.052
C
+/Y
-/Y
-/Y CDKL5
-/Y TATk-CDKL5
D
Spines/10µm
20
15
10
5
***
E
% mature spines
80
60
40
20
F
G
PSD-95 positive puncta/ µm2
1.2
0.9
0.6
0.3
H
+/Y
-/Y
-/Y CDKL5
-/Y TATk-CDKL5

Figure 4 Effect of CDKL5 and TATk-CDKL5 proteins on dendritic morphology and connectivity. (A,B) Apical and basal mean total dendritic length (A) and mean number of dendritic segments (B) of Golgi-stained CA1 pyramidal neurons of wild-type (+/Y, n = 3) and *Cdkl5* KO (-/Y, n = 3) mice and of *Cdkl5* -/Y mice 90 days from treatment with AAVPHP.B_CDKL5 (n = 4) or AAVPHP.B_Igk-TATk-CDKL5 (n = 4). (C) Example of the reconstructed apical and basal dendritic tree of Golgi-stained CA1 pyramidal neurons of 1 animal from each experimental group. Scale bar = 40 μm (D, E) Dendritic spine density (D) and percentage of mature spines in relation to the total number of protrusions (E) of CA1 pyramidal neurons from wild-type (+/Y, n = 3) and *Cdkl5* KO (-/Y, n = 3) mice and of *Cdkl5* -/Y mice treated with AAVPHP.B_CDKL5 (n = 4) or AAVPHP.B_Igk-TATk-CDKL5 (n = 4). (F) Images of Golgi-stained dendritic branches of CA1 pyramidal neurons of 1 animal from each experimental group. Scale bar = 2 μm. (G) Number of fluorescent puncta per μm^2 exhibiting PSD-95 immunoreactivity in the CA1 layer of the hippocampus of wild-type (+/Y, n = 3) and *Cdkl5* KO (-/Y, n = 3) mice and of *Cdkl5* -/Y mice treated with AAVPHP.B_CDKL5 (n = 4) or AAVPHP.B_Igk-TATk-CDKL5 (n = 4). (H) Representative fluorescence image of PSD-95 immunoreactive puncta in the hippocampus of 1 animal from each experimental group. Scale bar = 6 μm. Values are represented as means ± SE. *P< 0.05; **P < 0.01; ***P < 0.001 (datasets in A, B, D and G, Turkey's test after one-way ANOVA; dataset in E, Dunn's test after a Kruskal-Wallis test).

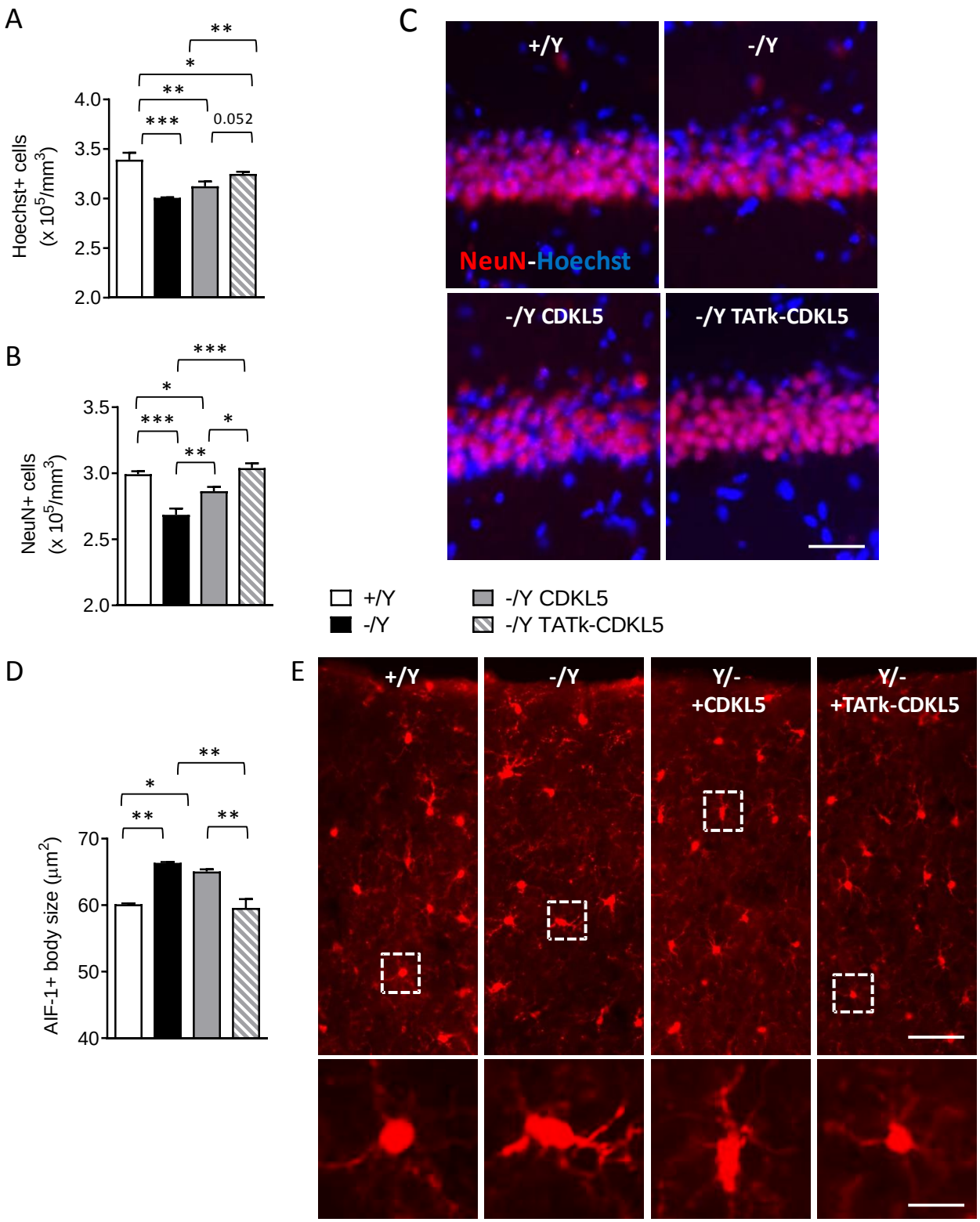

Figure 5. Effect of CDKL5 and TATk-CDKL5 proteins on neuronal survival and microglia activation in the brain of *Cdkl5* -/Y mice.

(A, B) Quantification of Hoechst-positive cells (A) and NeuN-positive cells (B) in the CA1 layer of hippocampal sections from wild-type (+/Y, n = 3) and Cdkl5 KO (-/Y, n = 3) mice and from *Cdkl5* -/Y mice treated with AAVPHP.B_CDKL5 (n = 4) or AAVPHP.B_Igk-TATk-CDKL5 (n = 4). (C) Representative fluorescence images of sections that were immunopositive for NeuN (red) and counterstained with

Hoechst (blue) in the hippocampal CA1 region of 1 animal from each group. Scale bar = 50 µm. (D) Mean microglia cell body size in cortical sections from wild-type (+/Y, n = 3) and *Cdkl5* KO (-/Y, n = 3) mice, and from Cdkl5 -/Y mice treated with AAVPHP.B_CDKL5 (n = 4) or AAVPHP.B_Igk-TATk-CDKL5 (n = 4). (E) Representative fluorescence images of cortical sections processed for AIF-1 immunohistochemistry of one animal from each group. The dotted boxes in the upper panels indicate microglial cells shown in magnification in the lower panels. Scale bar = 30 µm (low magnification), 10 µm (high magnification). Values are presented as means ± SE. *$p < 0.05$; **$p < 0.01$; ***$p < 0.001$ (Fisher's LSD test after one-way ANOVA).

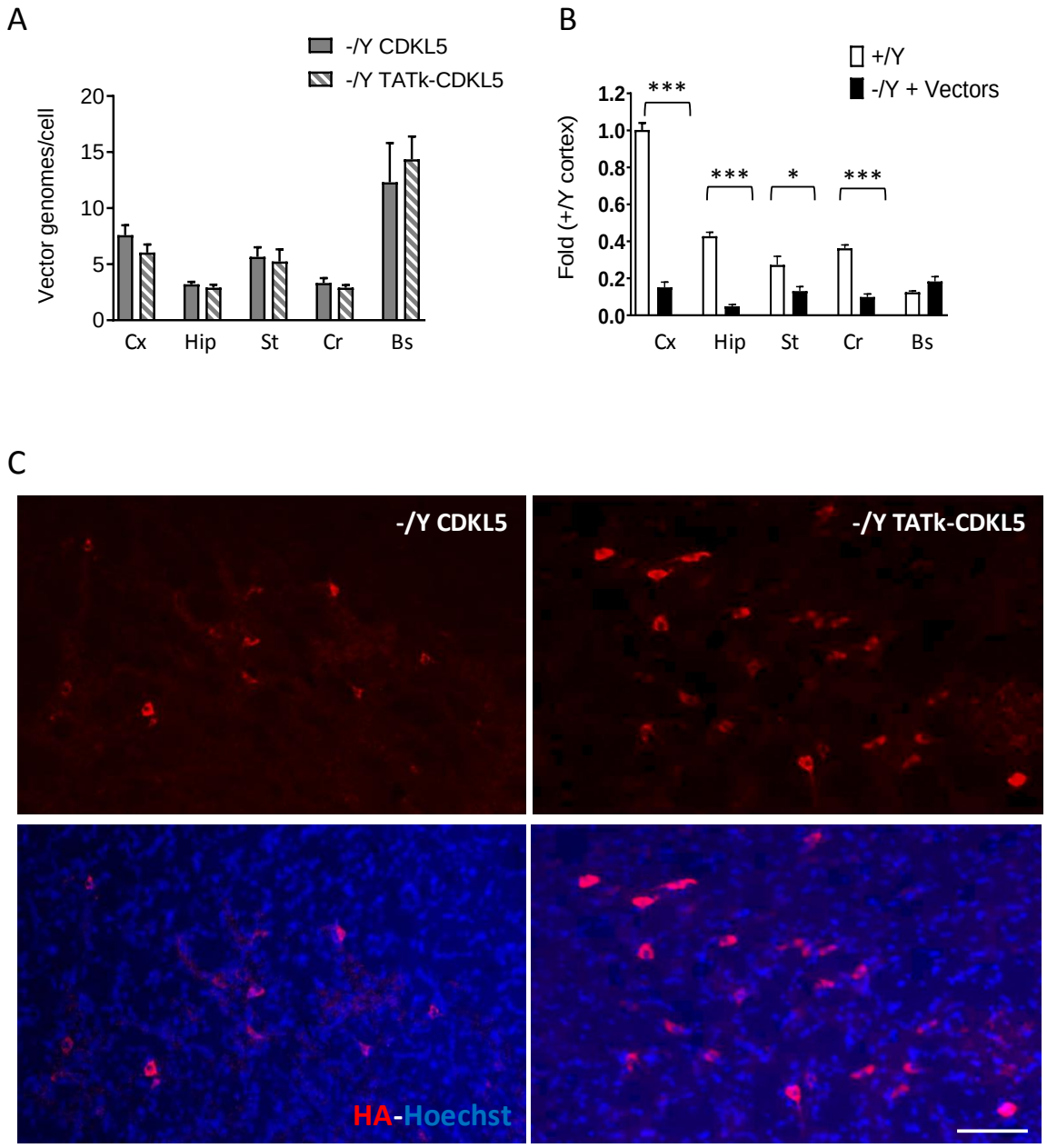

Figure 6. AAV vector transduction and expression and CDKL5 and TATk-CDKL5 protein in the CNS. (A) Vector genome copy numbers per diploid genomic equivalent in the cortex (Cx, n = 24), hippocampus (Hip, n = 16), striatum (St, n = 16), cerebellum (Cr, n = 24), and brainstem (Bs, n = 4) of *Cdkl5* -/Y mice treated with AAVPHP.B_CDKL5 or AAVPHP.B_Igk-TATk-CDKL5. (B) Expression of mRNA for CDKL5 in the cortex (Cx), hippocampus (Hip), striatum (St), cerebellum (Cr), and brainstem (Bs) of vehicle-treated wild-type mice (+/Y, n = 5) and of *Cdkl5* KO mice treated with AAVPHP.B vectors (AAVPHP.B_CDKL5 and AAVPHP.B_Igk-TATk-CDKL5; n = 9). Data are given as the fold change of the +/Y cortex. (C) CDKL5 and TATk-CDKL5 protein distribution in the CNS. Images show TATk-CDKL5 or CDKL5 protein localization in the striatum of treated mice 90 days post-injection. Localization of TATk-CDKL5 or CDKL5 was evaluated through immunohistochemistry using an anti-CDKL5 antibody, and nuclei were counterstained with Hoechst. Scale bar = 50 µm.